Monthly Notices of the ROYAL ASTRONOMICAL SOCIETY

MNRAS **428,** 2418–2429 (2013) doi:10.1093/mnras/sts201

Radio and γ-ray follow-up of the exceptionally high-activity state of PKS 1510−089 in 2011

M. Orienti,[1,2]★ S. Koyama,[3,4] F. D'Ammando,[2,5] M. Giroletti,[2] M. Kino,[3] H. Nagai,[3] T. Venturi,[2] D. Dallacasa,[1,2] G. Giovannini,[1,2] E. Angelakis,[6] L. Fuhrmann,[6] T. Hovatta,[7] W. Max-Moerbeck,[7] F. K. Schinzel,[8] K. Akiyama,[3,4]† K. Hada,[2] M. Honma,[3,9] K. Niinuma,[10] D. Gasparrini,[11] T. P. Krichbaum,[6] I. Nestoras,[6] A. C. S. Readhead,[7] J. L. Richards,[12] D. Riquelme,[13] A. Sievers,[13] H. Ungerechts[13] and J. A. Zensus[6]

[1]*Dipartimento di Astronomia, Università di Bologna, via Ranzani 1, I-40127 Bologna, Italy*
[2]*INAF – Istituto di Radioastronomia, via Gobetti 101, I-40129 Bologna, Italy*
[3]*National Astronomical Observatory of Japan 2-21-1 Osawa, Mitaka, Tokyo 181-8588, Japan*
[4]*Department of Astronomy, Graduate School of Science, The University of Tokyo, 7-3-1 Hongo, Bunkyo-ku, Tokyo 113-0033, Japan*
[5]*Dipartimento di Fisica, Universià degli Studi di Perugia, I-06123 Perugia, Italy*
[6]*Max-Planck-Institut für Radioastronomie, Auf dem Hügel 69, D-53121 Bonn, Germany*
[7]*Cahill Center for Astronomy and Astrophysics, California Institute of Technology 1200 E. California Blvd., Pasadena, CA 91125, USA*
[8]*Department of Physics and Astronomy, University of New Mexico, Albuquerque, NM 87131, USA*
[9]*Department of Astronomical Science, The Graduate University for Advanced Studies, 2-21-1 Osawa, Mitaka, Tokyo 181-8588, Japan*
[10]*Graduate School of Science and Engineering, Yamaguchi University, 1677-1 Yoshida, Yamaguchi, Yamaguchi 753-8512, Japan*
[11]*Agenzia Spaziale Italiana (ASI) Science Data Center, I-00044 Frascati (Roma), Italy*
[12]*Department of Physics, Purdue University, 525 Northwestern Avenue, West Lafayette, IN 47907, USA*
[13]*Instituto de Radioastronomía Millimétrica (IRAM), Avenida Divina Pastora 7, Local 20, E-18012 Granada, Spain*

Accepted 2012 October 12. Received 2012 October 5; in original form 2012 June 14

ABSTRACT

We investigate the radio and γ-ray variability of the flat spectrum radio quasar PKS 1510−089 in the time range between 2010 November and 2012 January. In this period the source showed an intense activity, with two major γ-ray flares detected in 2011 July and October. During the latter episode both the γ-ray and the radio flux density reached their historical peak. Multiwavelength analysis shows a rotation of about 380° of the optical polarization angle close in time with the rapid and strong γ-ray flare in 2011 July. An enhancement of the optical emission and an increase of the fractional polarization both in the optical and in radio bands are observed about three weeks later, close in time with another γ-ray outburst. On the other hand, after 2011 September a huge radio outburst has been detected, first in the millimetre regime followed with some time delay at centimetre down to decimetre wavelengths. This radio flare is characterized by a rising and a decaying stage, in agreement with the formation of a shock and its evolution, as a consequence of expansion and radiative cooling. If the γ-ray flare observed in 2011 October is related to this radio outburst, then this strongly indicates that the region responsible for the γ-ray variability is not within the broad line, but a few parsecs downstream along the jet.

Key words: radiation mechanisms: non-thermal – galaxies quasars: individual: PKS 1510−089 – radio continuum: general.

1 INTRODUCTION

Relativistic jets are one of the most powerful manifestations of the release of energy produced by supermassive black holes in active galactic nuclei (AGN). Their emission is observed across the

★E-mail: orienti@ira.inaf.it
†Research Fellow of the Japan Society for the Promotion of Science.

entire electromagnetic spectrum, from the radio band to γ rays, and it is due to relativistic particles producing synchrotron radiation in low-energy bands (from radio to optical/X-rays), which may also give rise to high-energy emission by inverse Compton processes. The discovery of γ-ray emission from relativistic jets in AGN represented a breakthrough in our understanding of the physical processes involved.

Important clues on the jet physics have been obtained by the study of the blazar population. Blazars are radio-loud AGN whose jet axis is closely aligned with our line of sight. In these objects the jet emission is highly amplified due to Doppler boosting effects, and a high level of variability is detected at all wavelengths. In particular, blazars with strong γ-ray emission are brighter and more luminous at radio frequencies (Kovalev et al. 2009), have faster jets (Lister et al. 2009a) and higher variability Doppler factors (Savolainen et al. 2010) with respect to those without significant γ-ray emission.

Despite decades of efforts, many aspects of the physics of relativistic jets remain elusive. In particular, the location and the mechanisms responsible for the high-energy emission and the connection of the variability at different wavelengths are among the greatest challenges in the study of AGN. Recently, observations performed with the Very Long Baseline Array (VLBA), which allow sub-milliarcsecond angular resolution, suggested that the region responsible for the high-energy emission is located downstream along the jet at a distance of a few parsecs from the central AGN (e.g. Larionov et al. 2008; Marscher et al. 2008; Leòn-Tavares et al. 2011). On the contrary, following the causality argument, the very short time-scale variability detected at γ rays may imply that high-energy emission is produced in a small region. If the size of the emitting region is related to the jet cross-sectional radius, this suggests a location within the broad-line region (BLR, < 1 pc) (e.g. Tavecchio et al. 2010). If we consider that the entire cross-section of the jet is responsible for the γ-ray emission, this scenario is rather difficult to reconcile with its location at a distance of several parsecs from the central black hole (e.g. Sikora et al. 2008; Marscher et al. 2010), unless the collimation angle of the jet is extremely small. For example, in the case of PKS 1510−089 Jorstad et al. (2005) derived a half-opening angle of $0.^{\circ}2$ and the corresponding radius of the jet cross-section at about 10 pc is $\sim 10^{17}$ cm (Marscher et al. 2010).

Another explanation may involve turbulence in the jet flow. Marscher (2011) suggested that a turbulent multizone model may be able to describe the high-energy emission produced along the jet, several parsecs away from the central engine. In this model, the short γ-ray variability may be caused by a turbulent jet plasma that passes through a standing shock along the jet.

Recent multiband studies of blazars suggested that the high-energy emitting region is at parsec-scale distances from the central black hole. For example, in the blazar OJ 287 two major outbursts at millimetre wavelengths from a jet feature occurred almost simultaneously with both optical and γ-ray flares, suggesting that radio, optical and γ-ray variabilities are produced in a single region along the jet located about 14 pc downstream from the central engine (Agudo et al. 2011a). Further evidence for a location of the high-energy variability at few parsecs from the BLR was provided by the study of the multiwavelength outbursts in the blazars AO 0235+164 and 3C 345 (Agudo et al. 2011b; Schinzel et al. 2012).

Among the blazar population, the flat spectrum radio quasar (FSRQ) PKS 1510−089 is one of the most active objects where quiescent periods are interspersed with high-activity states with abrupt flux density increase at all wavebands (e.g. Tornikoski et al. 1994; Jorstad et al. 2001; Venturi et al. 2001). PKS 1510−089 was discovered as a γ-ray source by EGRET, and it is one of the three FSRQs detected at very high energy ($E > 100$ GeV) by MAGIC and HESS (Wagner 2010; Cortina 2012). During the EGRET era the γ-ray emission of PKS 1510−089 was found to be only slightly variable (Hartman et al. 1999). However, since 2008 the source has entered a very active period and many rapid and intense flaring episodes have been detected by *AGILE* and *Fermi* (e.g. Pucella et al. 2008; D'Ammando et al. 2009, 2011; Abdo et al. 2010a). Moreover, the high variability level detected in γ rays has been observed across the entire electromagnetic spectrum. Optical and radio outbursts seem to follow the high-activity states in γ rays with time delays of a few days in the optical, up to a few months as we consider the longer wavelengths of the radio band (Abdo et al. 2010a). Furthermore the strong γ-ray flares observed in 2008 September and 2009 April are likely related to the ejection of a new superluminal jet component (Marscher et al. 2010). However, not all the γ-ray flares have the same characteristics in the various energy bands (e.g. D'Ammando et al. 2011) making the interpretation of the mechanism responsible for the high-energy emission not trivial.

Of particular interest is the second half of 2011, when some intense rapid γ-ray flares were detected. The first rapid flare was observed on July 4 by *AGILE* and *Fermi* (D'Ammando & Gasparrini 2011; Donnarumma et al. 2011). The second episode started on October 17 and reached the maximum on October 19 (Hungwe, Dutka & Ojha 2011). During the latter flare the source reached its highest γ-ray flux, becoming the second brightest AGN ever observed by *Fermi*.

Triggered by this extreme γ-ray activity, multifrequency radio Very Long Baseline Interferometry (VLBI) and single-dish observations in the centimetre and millimetre bands were performed. In this paper, we investigate the connection of the γ-ray activity detected by the *Fermi* gamma-ray space telescope with the emission at lower frequencies, focusing on the two main γ-ray flares which occurred in 2011 July and October.

The paper is organized as follows: in Section 2, we describe the radio data from VLBI Exploration of Radio Astrometry (VERA), VLBA, Medicina, F-GAMMA and Owens Valley Radio Observatory (OVRO) observations. In Section 3, we report the analysis of the *Fermi*-Large Area Telescope (LAT) data. In Section 4, we present the results of the radio and γ ray comparison, while discussion and concluding remarks are presented in Sections 5 and 6, respectively.

Throughout this paper, we assume the following cosmology: $H_0 = 71\,\mathrm{km\,s^{-1}\,Mpc^{-1}}$, $\Omega_\mathrm{M} = 0.27$ and $\Omega_\Lambda = 0.73$, in a flat Universe. At the redshift of the target, $z = 0.361$ (Thompson, Djorgovski & de Carvalho 1990), the luminosity distance D_L is 1913.2 Mpc, and 1 arcsec = 5.007 kpc.

2 RADIO DATA

2.1 VERA observations

From 2010 November to 2012 January, PKS 1510−089 was observed with four VERA stations at 22 GHz using the left-hand circular polarization feed only, typically twice per month, for a total of 32 observing epochs, within the framework of the Gamma-ray Emitting Notable-AGN monitoring by Japanese VLBI (GENJI) programme (for more details see Nagai et al. 2012a). Observations of PKS 1510−089 were spread into several scans of about 5 min each, for a total on-source observing time of about 15–30 min for each run.

Data reduction was performed using the NRAO's Astronomical Image Processing System (AIPS). A priori amplitude calibration was

Table 1. 22-GHz flux density of the core component measured by the VERA interferometer.

Obs. date	$S_{22\,\mathrm{GHz}}$ (Jy)	Obs. date	$S_{22\,\mathrm{GHz}}$ (Jy)
2010-11-01	2.03	2011-08-16	2.29
2010-11-10	1.78	2011-08-17	2.29
2010-11-18	1.83	2011-08-19	2.41
2010-11-29	1.70	2011-09-07	2.78
2010-12-04	1.62	2011-09-13	3.23
2010-12-13	1.56	2011-09-14	3.04
2010-12-14	1.47	2011-09-16	3.27
2011-01-22	1.97	2011-10-25	5.82
2011-02-11	1.84	2011-10-29	5.97
2011-02-26	2.25	2011-11-02	5.92
2011-04-11	1.57	2011-11-07	5.78
2011-04-25	1.40	2011-12-23	5.45
2011-05-12	1.50	2012-01-13	4.63
2011-05-23	1.59	2012-01-14	4.53
2011-08-14	2.22	2012-01-19	4.45
2011-08-15	2.37	2012-01-20	4.49

derived with the AIPS task APCAL on the basis of the measurements of the system temperatures and the antenna gain information for each VERA antenna. Uncertainties on the amplitude calibration are within 10 per cent. The source is strong enough to allow the fringe fitting with a solution interval of 1 min to preserve the phase coherence. Final images were produced after a number of phase self-calibration iterations. The flux density was derived by means of the AIPS task JMFIT which performs a Gaussian fit on the image plane. The typical resolution is about (1.5 × 1.0) mas. Total intensity flux densities are reported in Table 1.

2.2 MOJAVE data

We investigated the parsec-scale morphology and flux density variability at 15 GHz by means of 14-epoch VLBA data from the MOJAVE programme (Lister et al. 2009b). The data sets span the time interval between 2010 November and 2012 March. In addition, we included also observations performed in 2012 April and May, in order to better characterize the proper motion of the jet components likely ejected close in time with the γ-ray flares. We imported the calibrated uv data into the NRAO AIPS package. For a proper comparison with the VERA data, in addition to the *full-resolution* images, we produced also *low-resolution* images in total intensity considering the same uv range of the VERA data (i.e. from 50 to 170 Mλ) and the same resolution. To derive the polarization information we also produced Stokes' Q and U images. The flux density of the core region was derived by means of the AIPS task JMFIT which performs a Gaussian fit on the image plane. Total intensity flux density and polarization information are reported in Table 2.

2.3 Medicina observations

Since 2011 July, after the γ-ray flare detected by *Fermi*-LAT (D'Ammando & Gasparrini 2011), PKS 1510−089 has been monitored almost once per month with the Medicina single-dish telescope at 5 and 8.4 GHz. Observations have been performed with the new Enhanced Single-dish Control System (ESCS), which provides enhanced sensitivity and supports observations with the cross-scan technique. At each frequency the typical on source time is 40 s and the flux density was calibrated with respect to 3C 286. The flux densities at 5 and 8.4 GHz measured with the Medicina telescope are listed in Table 3.

Table 2. Flux density and polarization information of the central region of PKS 1510−089 from the MOJAVE 15-GHz VLBA data.

Obs. date	$S_{15\,\mathrm{GHz}}$ (mJy)	S_{p} (mJy)	χ (deg)
2010-11-29	1527	31 (2.0 per cent)	75
2010-12-24	1422	16 (1.1 per cent)	65
2011-02-20	1984	13 (0.7 per cent)	50
2011-02-27	1980	14 (0.7 per cent)	50
2011-03-05	2067	23 (1.1 per cent)	85
2011-05-21	1399	10 (0.7 per cent)	45
2011-07-24	1741	29 (1.7 per cent)	45
2011-08-26	2186	26 (1.2 per cent)	40
2011-10-03	3969	20 (0.5 per cent)	55
2011-12-12	6536	93 (1.4 per cent)	65
2011-12-29	6207	172 (2.8 per cent)	60
2012-01-14	5458	167 (3.0 per cent)	55
2012-03-04	4802	98 (2.0 per cent)	50
2012-03-27	4758	128 (2.7 per cent)	24

Table 3. Results of the Medicina 32-m radio telescope.

Obs. date	$S_{5\,\mathrm{GHz}}$	$S_{8.4\,\mathrm{GHz}}$
2011-07-12	–	1.30 ± 0.05
2011-08-10	1.38 ± 0.05	–
2011-09-08	1.36 ± 0.11	1.44 ± 0.11
2011-09-22	1.46 ± 0.07	1.82 ± 0.20
2011-10-13	1.53 ± 0.05	2.08 ± 0.05
2011-11-16	2.49 ± 0.17	3.72 ± 0.22
2011-12-01	2.85 ± 0.15	4.10 ± 0.15
2011-12-13	3.34 ± 0.12	4.59 ± 0.15
2012-01-03	3.70 ± 0.20	5.30 ± 0.40
2012-01-17	4.30 ± 0.20	–

2.4 F-GAMMA observations

The cm/mm radio light curves of PKS 1510−089 have been obtained within the framework of a *Fermi*-related monitoring programme of γ-ray blazars (F-GAMMA programme; Fuhrmann et al. 2007, Angelakis et al. 2008). The millimetre observations are closely coordinated with the more general flux monitoring conducted by IRAM, and data from both programmes are included in this paper. The overall frequency range spans from 2.64 to 142 GHz using the Effelsberg 100-m and IRAM 30-m telescopes and observations are performed roughly once per month.

The Effelsberg measurements were conducted with the secondary focus heterodyne receivers at 2.64, 4.85, 8.35, 10.45, 14.60, 23.05 and 32.0 GHz. The observations were performed quasi-simultaneously with cross-scans, which are slewing over the source position, in azimuth and elevation directions with adaptive number of sub-scans for reaching the desired sensitivity (for details see Angelakis et al. 2008; Fuhrmann et al. 2008). Pointing offset correction, gain correction, atmospheric opacity correction and sensitivity correction have been applied to the data.

The IRAM 30-m observations were carried out with calibrated cross-scans using the new EMIR horizontal and vertical polarization receivers operating at 86.2 and 142.3 GHz. The opacity-corrected intensities were converted into the standard temperature scale and

finally corrected for small remaining pointing offsets and systematic gain-elevation effects. The conversion to the standard flux density scale was done using the instantaneous conversion factors derived from frequently observed primary (Mars, Uranus) and secondary [W3(OH), K3-50A, NGC 7027] calibrators.

2.5 OVRO observations

PKS 1510−089 is part of an ongoing blazar monitoring programme at 15 GHz, the OVRO 40-m radio telescope. This monitoring programme includes over 1500 confirmed and candidate γ-ray-loud blazars above declination -20° (Richards et al. 2011). The sources in this programme are observed in total intensity twice per week with a 4 mJy (minimum) and 3 per cent (typical) uncertainty. Observations are performed with a dual-beam (each 2.5 arcmin FWHM) Dicke-switched system using cold sky in the off-source beam as the reference. Additionally, the source is switched between beams to reduce atmospheric variations. The absolute flux density scale is calibrated using observations of 3C 286, adopting the flux density (3.44 Jy) from Baars et al. (1977). This results in about a 5 per cent absolute scale uncertainty, which is not reflected in the plotted errors.

3 *Fermi*-LAT DATA: SELECTION AND ANALYSIS

The LAT onboard *Fermi* is a γ-ray telescope operating from 20 MeV to >300 GeV. The instrument is an array of 4 × 4 identical towers, each one consisting of a tracker (where the photons are pair-converted) and a calorimeter (where the energies of the pair-converted photons are measured). The entire instrument is covered with an anticoincidence detector to reject the charged-particle background. The LAT has a large peak effective area (∼8000 cm^2 for 1 GeV photons), an energy resolution typically about 10 per cent and a field of view of about 2.4 sr with an angular resolution (68 per cent containment angle) better than 1° for energies above 1 GeV. Further details about the LAT are given by Atwood et al. (2009).

The LAT data reported in this paper were collected over 15 months of *Fermi* operation, from 2010 November 1 (MJD 555 01) to 2012 January 31 (MJD 559 57). During this time the LAT instrument operated almost entirely in survey mode. The analysis was performed with the SCIENCETOOLS software package version v9r23p1. The LAT data were extracted within a 15° region of interest (RoI) centred at the radio location of PKS 1510−089. Only events belonging to the 'Source' class were used. In addition, a cut on the zenith angle[1] (<100°) was also applied to reduce contamination from the Earth limb γ rays, which are produced by cosmic rays interacting with the upper atmosphere. The spectral analysis (from which we derived spectral fits and photon fluxes) were performed with the post-launch instrument response functions P7SOURCE_V6 using an unbinned maximum likelihood method implemented in the Science tool `gtlike`.

The background model used to extract the γ-ray signal includes a Galactic diffuse emission component and an isotropic component. The model that we adopted for the Galactic component is given by the file gal_2yearp7v6_v0.fits and the isotropic component, which is the sum of the extragalactic diffuse emission and the residual charged-particle background, is parametrized by the file iso_p7v6source.txt.[2] The normalizations of both components in the background model were allowed to vary freely during the spectral point fitting.

We examine the significance of the γ-ray signal from the sources by means of the test statistics (TS) based on the likelihood ratio test. The TS = 2Δlog(likelihood) between models with and without the source is a measure of the probability of having a γ-ray source at the localization specified, which compares models whose parameters have been adjusted to maximize the likelihood of the data given the model (Mattox et al. 1996). The source model used in `gtlike` includes all the point sources from the second *Fermi*-LAT catalogue (2FGL; Nolan et al. 2012) that fall within 20° from PKS 1510−089. In addition in the model we included also the FSRQ TXS 1530−131, at 6° from the source, detected in flare by *Fermi*-LAT on 2011 August 22 (Gasparrini & Cutini 2011). The spectra of these sources were parametrized by power-law functions, except for 2FGL J1504.3+1029, for which we used a log-parabola for its spectral modelling as in the 2FGL catalogue. We removed from the model the sources having TS < 25 and/or fluxes below 1.0×10^{-8} photons cm^{-2} s^{-1} over 15 months and repeated the fit. Thus, a final fitting procedure has been performed with the sources within 10° from PKS 1510−089 included with the normalization factors and the photon indices left as free parameters. For the sources located between 10° and 15°, we kept the normalization and the photon index fixed to the values obtained in the previous fitting procedure. The RoI model includes also sources at distances between 15° and 20° from the target source, which can contribute to the total counts observed in the RoI due to the energy-dependent size of the point spread function of the instrument. For these additional sources, normalizations and indices were fixed to the values of the 2FGL catalogue.

Following the 2FGL catalogue the spectral model used for PKS 1510−089 is a log-parabola, $\mathrm{d}N/\mathrm{d}E \propto E/E_0^{-\alpha-\beta\,\log(E/E_0)}$ (Landau et al. 1986; Massaro et al. 2004), where the parameter α is the spectral slope at the energy E_0 and the parameter β measures the curvature around the peak. We fixed the reference energy E_0 to 259.6 MeV as in the 2FGL catalogue. The fit over the entire period from 2010 November to 2012 January (MJD 555 01–559 57) in the 0.1–100 GeV energy range results in a TS = 20 678, with $\alpha = 2.22 \pm 0.02$, $\beta = 0.07 \pm 0.01$, and an integrated average flux of $(88.3 \pm 1.4) \times 10^{-8}$ photons cm^{-2} s^{-1}. Using a power-law model the fit yielded to a TS = 20 155, with a photon index $\Gamma = 2.33 \pm 0.02$ and an integrated average flux of $(90.1 \pm 1.3) \times 10^{-8}$ photons cm^{-2} s^{-1}, corresponding to an isotropic γ-ray luminosity of $\sim 1.6 \times 10^{47}$ erg s^{-1}. As a comparison the isotropic γ-ray luminosity over the first 2 yr of *Fermi* operation is $\sim 1.8 \times 10^{47}$ erg s^{-1}, indicating that the source activity remained quite high throughout the *Fermi* era.

Fig. 1 shows the *Fermi*-LAT γ-ray light curve of PKS 1510−089 during the 15 months considered in this paper using one-week time bins and the log-parabola spectral model. For each time bin the α and β parameters were frozen to the value resulting from the likelihood analysis over the entire period. If TS < 10, the values of the fluxes were replaced by the 2σ upper limits. The systematic uncertainty in the flux is energy dependent: it amounts to 10 per cent at 100 MeV, decreasing to 5 per cent at 560 MeV and increasing to 10 per cent above 10 GeV (Ackermann et al. 2012).

Several prominent γ-ray peaks are clearly visible in the one-week light curve over 15 months. We produced two additional light curves

[1] The zenith angle is defined as the angle of a photon's apparent origin to the Earth-spacecraft vector.

[2] http://fermi.gsfc.nasa.gov/ssc/data/access/lat/BackgroundModels.html

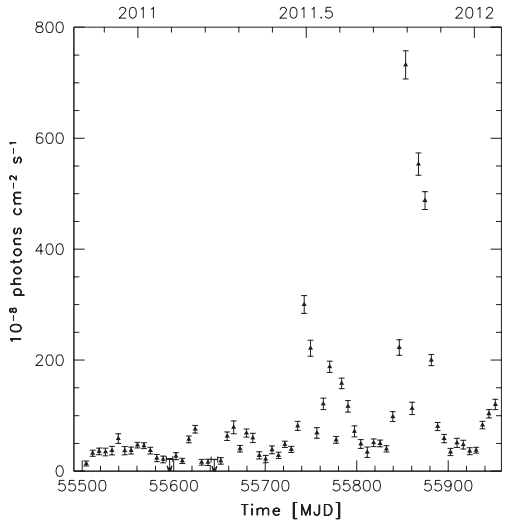

Figure 1. *Fermi*-LAT integrated flux (E > 100 MeV) light curve of PKS 1510−089 obtained from 2010 November 1 (MJD 555 01) to 2012 January 31 (MJD 559 57) using one-week time bins. The arrows refer to 2σ upper limit on the source flux. The upper limits are computed when TS < 10.

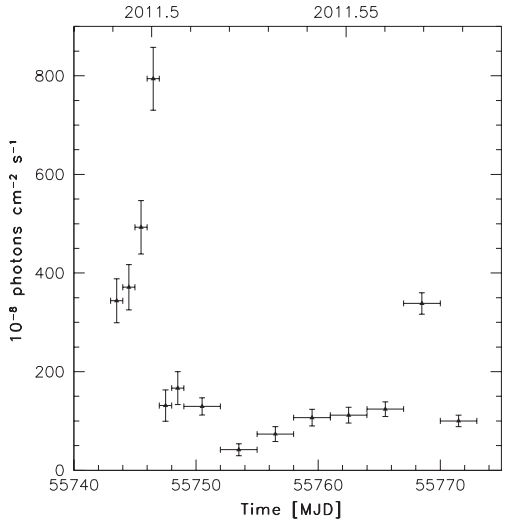

Figure 2. Integrated flux (E > 100 MeV) light curve of PKS 1510−089 obtained from 2011 July 1 to 30 (MJD 557 43–557 73) with either 1-d (close to peak) or 3-d time bins.

focused on the periods when the largest flares occurred: 2011 July 1 to 30 (MJD 557 43–557 73) and 2011 October 3 to November 28 (MJD 558 37–558 93), using the log-parabola spectral model with either 1-d (close to the peaks, corresponding to the time bins with higher statistics) or 3-d time bins (Figs 2 and 3). The 2011 July and October flares are characterized by a doubling time-scale ($t_{\rm var}$) of 2 and 1 d, respectively. The daily peak isotropic γ-ray luminosities are 1.6×10^{48} erg s^{-1} on July 4, 3.7×10^{48} erg s^{-1} on October 19 and 2.3×10^{48} erg s^{-1} on November 2, with an increase of a factor of 10, 23 and 14, with respect to the average value. To calculate these values we used the photon index obtained from a power-law model estimated over the relative one-week time bin: $\Gamma_{\rm July} = 2.21 \pm 0.05$, $\Gamma_{\rm October} = 2.09 \pm 0.03$ and $\Gamma_{\rm November} = 2.26 \pm 0.04$, respectively.

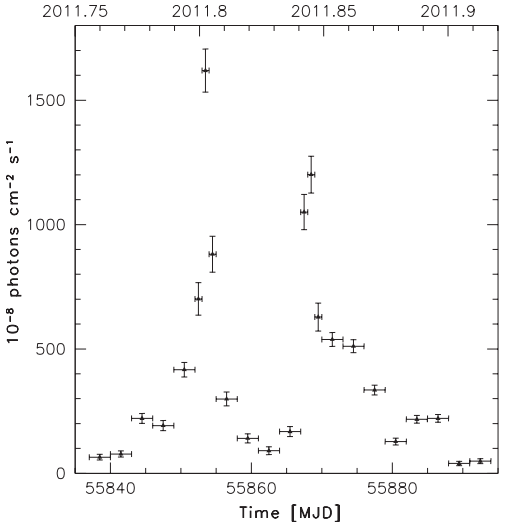

Figure 3. Integrated flux (E > 100 MeV) light curve of PKS 1510−089 obtained from 2011 October 3 to November 28 (MJD 558 37–558 93) with either 1-d (close to the peak) or 3-d time bins.

4 RESULTS

4.1 Light curves

In 2011, PKS 1510−089 showed high activity in the γ-ray energy band, with an average weekly flux between 100 MeV and 100 GeV of about 8×10^{-7} photons cm^{-2} s^{-1} (Fig. 1). The second-half of 2011 is characterized by two major flares which occurred in July (Fig. 2) and October (Fig. 3).

To compare the flux variability at high (γ rays) and low (radio band) energies, we analysed millimetre/centimetre radio observations spanning a time interval between 2010 November and 2012 January, i.e. long enough to constrain any flux density variation well before and after the main γ-ray outbursts. In Fig. 4, we plot the radio light curves at 23 and 15 GHz, i.e. those frequencies with the best time sampling. The light curves are characterized by subsequent increase and decrease of the flux density. Since 2011 September the flux density at both 15 and 23 GHz abruptly increased, reaching its maximum at the beginning of November for the 23 GHz, followed with one-month delay at 15 GHz, when the peak was observed around middle of December. It is worth noting that the flux density on parsec scales derived by VLBI data, i.e. VERA data at 22 GHz and VLBA data at 15 GHz (triangles and stars in Fig. 4) strictly follow the single-dish flux density trend, indicating that the flux density variability is dominated by the parsec-scale emitting region.

In Fig. 5, we report the multifrequency light curves from 2.6 to 142 GHz, in order to compare the flux density behaviour at various frequencies. The abrupt flux density increase reported since the beginning of September (Nestoras et al. 2011) is first detected above 22 GHz. At these frequencies the light curves show a structure similar to a plateau starting from the time of the October γ-ray flare. At lower frequencies the flux density increase is much smoother and with some time delay (Orienti et al. 2011a).

4.2 Time delay

Statistical studies of the light curves of blazars showed that the maximum flux density value reached during an outburst strictly depends on the observing frequency and usually it is not simultaneous

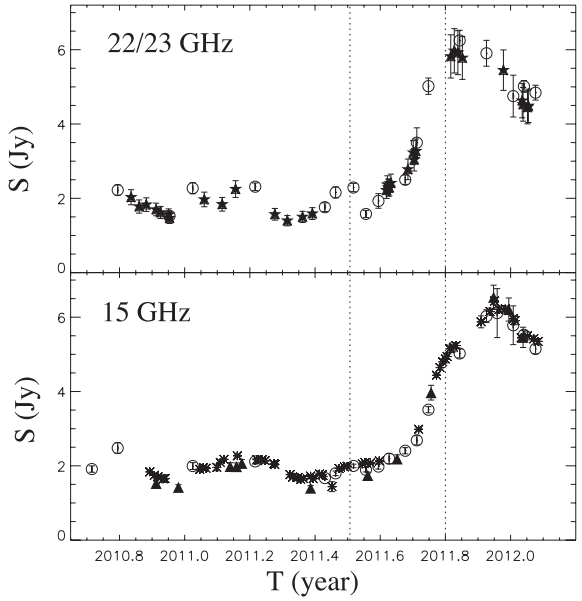

Figure 4. Radio light curves at 22 and 23 (*upper panel*) and 15 GHz (*lower panel*) of PKS 1510−089. The empty circles are F-GAMMA data at 15 and 23 GHz; the filled stars are VERA data at 22 GHz, the asterisks and the filled triangles represent, respectively, OVRO and MOJAVE data at 15 GHz. The vertical lines indicate the time of the γ-ray flares.

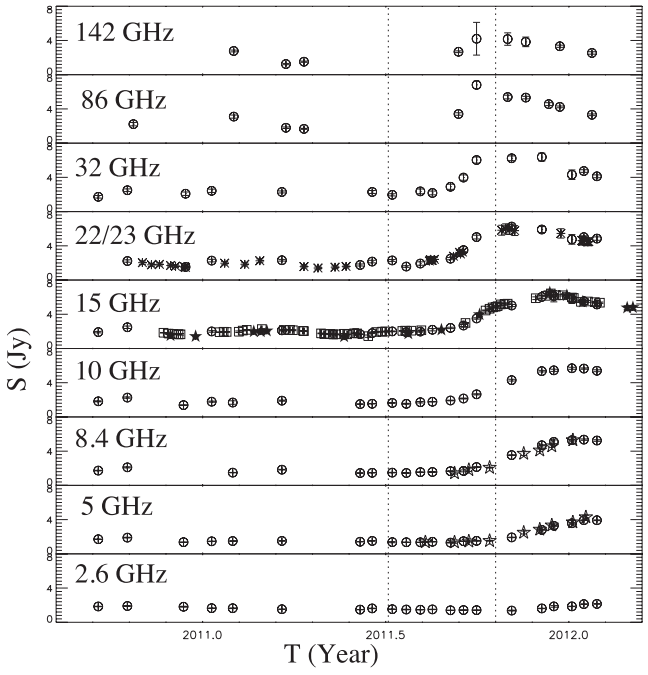

Figure 5. Radio light curves of PKS 1510−089 between 2010 November 1 and 2012 January 31. The circles, asterisks, squares, filled stars and empty stars refer to F-GAMMA data, 22-GHz VERA data, 15-GHz OVRO data, 15-GHz MOJAVE data and Medicina data, respectively. The vertical lines indicate the time of the γ-ray flares.

at the various frequencies (e.g. Hovatta et al. 2008; Hughes, Aller & Aller 2011). In the shock scenario we expect that the peak occurs first in the millimetre regime then followed with some time delay at the longer wavelengths, as a consequence of jet opacity. Time lags between frequencies are thus important to constrain the properties of the shock at the origin of the observed outburst.

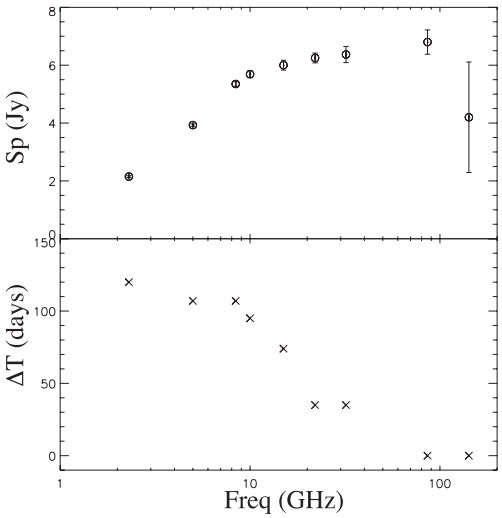

Figure 6. Peak flux density (*top*) and the time delay between burst maxima (*bottom*), normalized at the 86-GHz values, against the observing frequency.

The main problem in determining the characteristics of the light curves depends on the time sampling of the observations at each frequency: if observations are too sparse in time, the epochs at which the flux density starts to rise and then peaks cannot be constrained with adequate accuracy, causing large uncertainties on the parameters of the shock. This is particularly critical at high frequencies where the variability is faster and the atmosphere is more incoherent, making the measurements more difficult and with larger uncertainties.

The analysis of the multifrequency light curves clearly indicates that at the highest frequencies, 86 and 142 GHz, the flux density reaches its maximum almost simultaneously at the end of September, while at longer wavelengths it occurs after some time delay (Fig. 5). In Fig. 6, we report the peak flux density (*upper panel*) and the time lag (*lower panel*), normalized at the 86 GHz values, as a function of the frequency. The time delay increases with the wavelengths, from about one month at 32 and 22 GHz, up to several months in the decimetre regime (at 2.6 GHz). Although the peak at 86 and 142 GHz seems to precede the high γ-ray flare detected in October, the actual peak time could have been missed during observations due to the sparse time coverage. For this reason, we cannot exclude a simultaneity between the millimetre peak and the γ-ray flare. It is worth noting that the flux density increase observed since 2011 September might be related to the γ-ray flare detected in 2011 July. However, flares at millimetre wavelengths often peak quasi-simultaneously with the γ-ray flare (Abdo et al. 2010a), and a delay of almost three months at millimetre wavelengths is unusual. As a comparison, we note that during the high-activity states showed by PKS 1510−089 in the first-half of 2009, the peak at 230 GHz occurred about one month after the γ-ray flare observed in 2009 March, and almost simultaneously with the γ-ray flare detected in 2009 April (Abdo et al. 2010a).

Following the approach discussed by Valtaoja et al. (1992) we computed the maximum relative flux density scaled to the frequency at which the maximum occurs (Fig. 7). Since the maximum peak flux density seems to be at 86 GHz, we normalized the values to this frequency. In the shock scenario we expect three different evolutionary epochs: (1) the growth stage at high frequencies, where the radiation is optically thin, (2) a plateau stage, where the turnover frequency moves towards lower frequencies while the peak flux

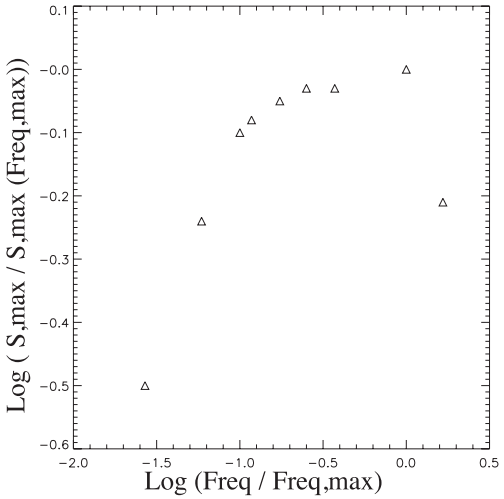

Figure 7. Observed maximum relative flux density scaled to the frequency at which the maximum occurs.

density is almost constant and (3) a decay stage at low frequencies, where the peak flux density is lower than in the plateau stage due to strong energy losses. To study the evolutionary stages of the outburst that took place in 2011 October, we fit the three parts of the normalized spectrum with a power law (Fig. 7). We find a slope of 0.5 and −0.9 for the declining (between 10 and 5 GHz) and the rising part (between 142 and 86 GHz), respectively, and 0.06 for the plateau (between 86 and 15 GHz). The slope of the declining part has been computed considering the 5 GHz as the lowest frequency, since at 2.6 GHz the flux density is still increasing in 2012 January. The rising part is not well constrained due to the poor time sampling and the large uncertainty on the flux density.

4.3 Parsec-scale properties

Single-dish observations cannot separate the various contributions to the emission and the flux density variability originating in the central region, as well as its polarization properties, may be washed out. Observations with parsec-scale resolution are required to disentangle the contribution of the core region from the emission arising from the jet and extended features.

On the parsec scale, the radio emission from PKS 1510−089 is dominated by the core component, from which the jet emerges with a position angle of ∼−35°, i.e. to the north-west direction (Fig. 8). Fig. 9 shows the radio properties of the parsec-scale core region obtained by means of high-resolution VLBA observations at 15 GHz. As pointed out in Section 4.1 the variability shown by the source clearly originates in the core region. The core light curve shows a strong increase starting from 2011 September. Simultaneously, the polarization percentage of the core decreases, while the polarization angle remains almost constant. After the γ-ray flare in 2011 October, the fractional polarization increases from ∼0.5 per cent of October, with a polarized flux density of 20 mJy, to ∼3.0 per cent measured in 2012 January, when the polarized emission reached ∼170 mJy. On the other hand, no significant changes were observed in the electric vector position angle (EVPA), which ranges between 55° and 65° in the same period.

The analysis of the multiepoch parsec-scale morphology of PKS 1510−089 points out that the jet component, labelled 'J' in Fig. 8, is moving outwards from the core. To determine the proper motion of the jet component we model-fitted the visibility data of each

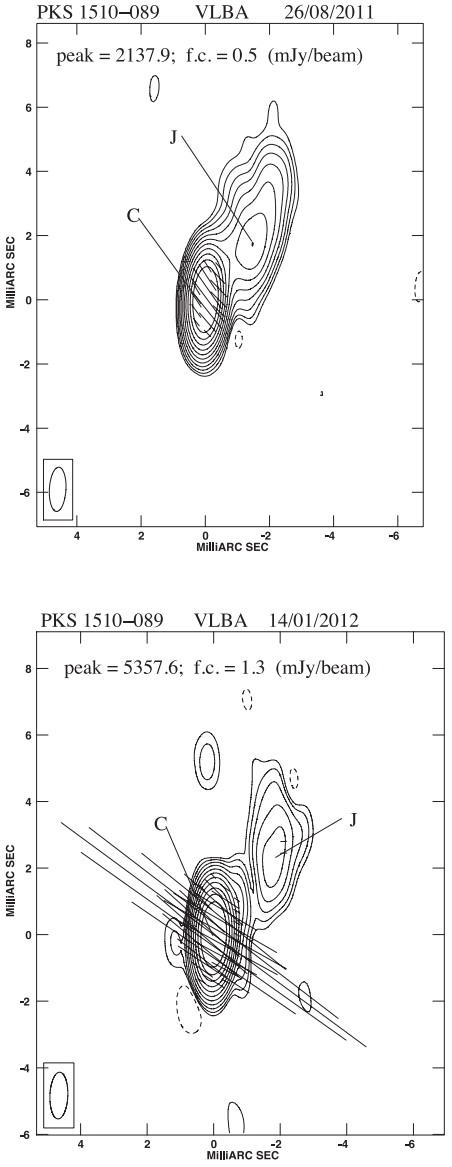

Figure 8. 15-GHz VLBA images of PKS 1510−089 relative to 2011 August (*upper panel*) and 2012 January (*bottom panel*). On each image, we provide the telescope array and the observing date; the peak flux density is in mJy/beam and the first contour (f.c.) intensity is in mJy/beam, which corresponds to three times the off-source noise level. Contour levels increase by a factor of 2. The restoring beam is plotted in the bottom-left corner. For the data sets with polarization information, the vectors superimposed on the I contours show the position angle of the E vector, where 1 mas length corresponds to 14.3 mJy/beam.

observing epoch with Gaussian components using the model-fitting option in `DIFMAP` (for a description of the model-fitting procedure and the associated errors see Orienti et al. 2011b). We performed the study of the source structure using 15-GHz VLBA data from the MOJAVE programme, since both the uv coverage and the sensitivity of the 22-GHz VERA data are not adequate.

The angular separation velocity and time of zero separation (T_0) from the core were derived by means of a linear fit. In addition to the 16 MOJAVE epochs considered in this paper, we also fit earlier epochs already published in Orienti et al. (2011b). From this analysis we found that component J, labelled 'N3' in Orienti et al. (2011b), is separating from the core with an angular velocity of

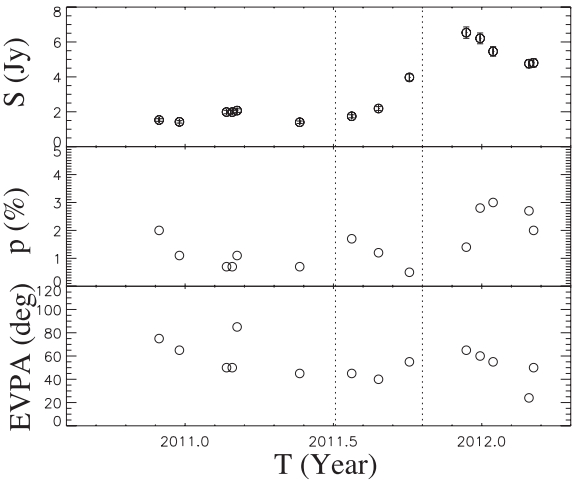

Figure 9. Total intensity and polarization properties of the core region of PKS 1510−089 at 15 GHz. From top to bottom panel: total intensity flux density; polarization percentage; polarization angle. The vertical lines indicate the time of the γ-ray flares.

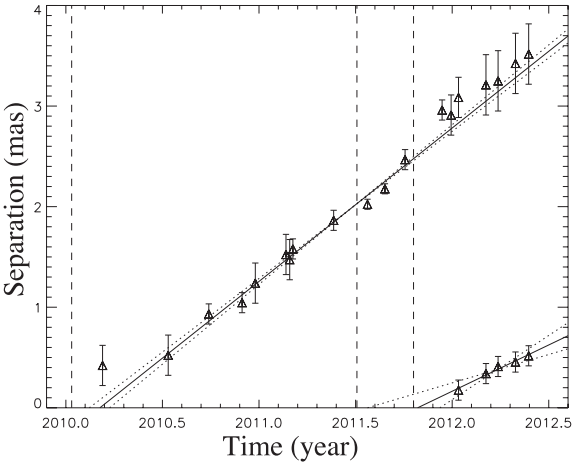

Figure 10. Changes in separation with time between components C, considered stationary, J, and the new knot ejected in 2011. The solid line represents the regression fit to the 15-GHz VLBA data, while the dashed lines represent the uncertainties from the fit parameters. Dashed vertical lines indicate the time of the γ-ray flares.

1.5 ± 0.1 mas yr^{-1}, which corresponds to an apparent velocity of $(33.4 \pm 2.2)c$ (Fig. 10). This value is larger than what was found by Orienti et al. (2011b) based on five epochs only. The availability of additional 16 observing epochs allows a more accurate estimate of the proper motion. The time of zero separation is 2010.18 ± 0.05, in agreement with the previous estimate. Interestingly, the ejection of this component is close in time with a γ-ray flare detected by *AGILE* in 2010 January (Striani et al. 2010).

The model fit of the MOJAVE data sets did not reveal the ejection of a new component until 2012 January. After this time the observations show the presence of a new feature that is moving away from the core. A linear fit of the five epochs in which the new component is detected (i.e. from 2012 January to May) provides an angular separation rate of 0.92 ± 0.35 mas yr^{-1}, which corresponds to an apparent separation velocity of $(20.5 \pm 7.8)c$. From the regression fit we estimate that the time of zero separation occurred about 2011.83 (i.e. October 26), making the ejection of the blob close in time with the γ-ray flare detected in 2011 October. However, the large uncertainties due to the availability of a few epochs spanning a short time range do not allow us to accurately constrain the precise time of zero separation, which ranges between 2011.56 (i.e. July 23) and 2011.93 (i.e. December 5). Although the typical apparent speed measured for PKS 1510−089 is usually larger than $15c$ supporting the idea that the new jet component is related to the October γ-ray flare, we cannot exclude that its ejection occurred close in time with the 2011 July outburst.

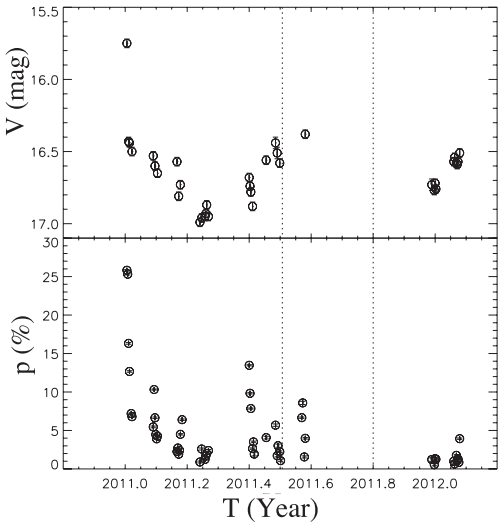

Figure 11. Optical *V*-band light curve (*top*) and polarization percentage (*bottom*) of PKS 1510−089 between 2011 January and 2012 January. The vertical lines indicate the time of the γ-ray flares.

4.4 Optical emission

Previous multifrequency studies of PKS 1510−089 showed an irregular flux variability between γ-ray and optical emission. D'Ammando et al. (2011) found that during the high activity of 2009 March, the optical outburst occurred with about 1-d lag with respect to the γ-ray flare. On the other hand, a lag of 13 ± 1 d between the γ-ray and the optical peaks was reported in Abdo et al. (2010a) for the 2009 January and April flares. Furthermore, in the same period the strong γ-ray flare that took place in 2009 April seems to coincide with the end of a 50-d rotation of the optical polarization angle, suggesting a connection between these two energy bands (Marscher et al. 2010).

To test possible connection between the γ-ray flaring events with changes in the optical emission we make use of the optical data from the Steward Observatory blazar monitoring programme of the University of Arizona.[3] A description of this monitoring project, the calibration and the data products can be found in Smith et al. (2009).

In Fig. 11, we show the *V*-band light curve and the polarization percentage (λ = 500–700 nm). The mean *V*-band magnitude is 16.65, while the mean polarization percentage is ∼5 per cent. No obvious trend between the optical emission and the fractional polarization has been found.

Interestingly, no significant increase in the optical luminosity has been detected just after the γ-ray flare observed in 2011 July. At the beginning of July the magnitude was ∼16.6 and the polarized

[3] http://james.as.arizona.edu/∼psmith/Fermi

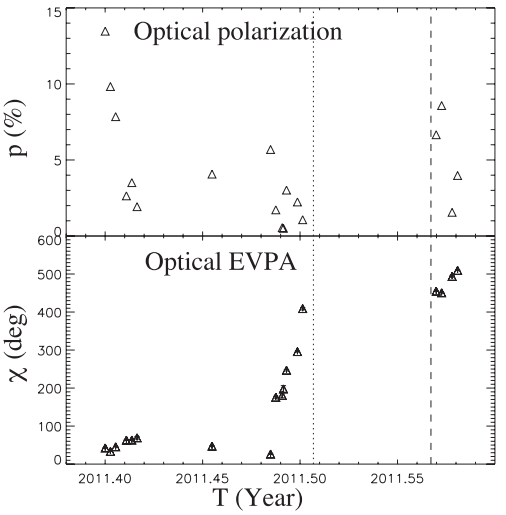

Figure 12. Optical polarization percentage (*top*) and EVPA of the optical polarization ($\lambda = 500$–700 nm) of PKS 1510−089 between 2011 May and July. The vertical lines indicate the time of the strong γ-ray flare of 2011 July 4 (*dotted line*) and the *R*-band flare (*dashed line*) detected between 2011 July 24 and 26 (Hauser et al. 2011). Multiples of 180° are added to EVPA as needed to minimize the jumps in consecutive values.

percentage was ∼1 per cent, well below the mean value. This result is in agreement with observations in *R*-band performed a few days after the γ-ray flare, where the optical emission ($R \sim 16.1$) is consistent with a low-activity state (Bachev et al. 2011). However, the γ-ray flare occurred close in time with the end of a 7-d period during which the optical polarization vector rotates of about 380° (Fig. 12). The beginning of the rotation of the optical polarization vector coincides with a local maximum in the percentage of polarization, which was about 5.7 per cent, while the *V*-band magnitude was 16.4. The polarization percentage dropped during the rotation, and it slightly increased at the end of the period. The lack of observations after July 2 do not allow us to describe the polarization trends soon afterwards the γ-ray flare.

An increase in both the optical emission and fractional polarization is detected a few weeks later, at the end of July, when the *V* magnitude reached 16.4. The polarized emission increased up to 8.6 per cent and the optical polarization angle rotates of about 60° in a 4-d period. This optical outburst was more prominent in the *R*-band, where the source magnitude reached 15.3 (Hauser et al. 2011). This event occurred close in time with an enhancement of the γ-ray flux (Fig. 2), and an increase of the radio polarization percentage, while the radio polarization angle does not show significant variation remaining stable between 40° and 60° (Fig. 8).

Unfortunately, during the huge γ-ray flare occurred in 2011 October the source was not observable in the optical and so no information is available.

It is interesting to note the presence of an optical flare at the beginning of 2011 January, when the *V*-band emission reached a magnitude of 15.75 and the fractional polarization was about 25 per cent. Then both the optical emission and polarization decreased reaching a *V*-band magnitude of about 16.5 and a polarization percentage of 6.8 per cent. During this 7-d period the optical polarization angle rotates of about 40°. Although no high γ-ray activity was detected in this period, the optical flare is close in time with a local maximum in the 22-GHz light curve (Fig. 4).

5 DISCUSSION

Multiwavelength monitoring campaigns suggest a relation between γ-ray flares and the radio variability, explained in terms of a shock moving along the jet, whose manifestation is a superluminal knot observable with high-frequency VLBI observations (e.g. Marscher & Gear 1985; Valtaoja et al. 1992; Hughes et al. 2011). The shock model implies: (1) a growth stage, when the shock forms up to the development of its maximum, which is observed not simultaneously at the various energy bands due to opacity effects (Compton losses dominate); (2) a plateau, when energy losses and gains are balanced (synchrotron losses dominate); (3) a decaying stage, when the shock fades due to energy losses (adiabatic losses dominate). However, not all the outbursts, even produced in the same source, behave similarly. For example, not all the γ-ray flares show a counterpart in the various energy bands. A clear example is represented by 3C 279 whose prominent γ-ray flare detected in 2009 February, and associated with changes in the optical flux and polarization angle, is not related to any variability in the radio band, even considering some time delay (Abdo et al. 2010b). A similar case is represented by the misaligned object 3C 84 where two major γ-ray flares detected by *Fermi*-LAT and MAGIC do not have an apparent counterpart in the radio band (Nagai et al. 2012b).

The FSRQ PKS 1510−089 is one of those objects which does not show a trivial connection between the light-curves behaviour at the various frequencies during different outbursts.

5.1 The high-activity state in 2011

In the second-half of 2011, PKS 1510−089 became very active, with two main flaring episodes occurring in July and October, with a daily isotropic peak luminosity above 10^{48} erg s^{-1}. The γ-ray light curve clearly shows the abrupt increase of the flux associated with the two prominent flares, both characterized by short time variability $t_{\rm var}$. Contrary to what was observed in the case of the FSRQ 3C 454.3 (e.g. Abdo et al. 2011c), the γ-ray flares of PKS 1510−089 are not preceded by a plateau in the γ-ray light curve, confirming the trend observed during previous flaring episodes for this source.

On the basis of the short time variability observed, we constrain the intrinsic size of the γ-ray emitting region R by means of the causality argument:

$$R \leq c t_{\rm var} \frac{\delta}{(1+z)}, \quad (1)$$

where δ is the relativistic Doppler factor and z is the redshift. Assuming $\delta = 20$, as typically found for this source (e.g. D'Ammando et al. 2009; Abdo et al. 2010a), and $t_{\rm var}$ of 2 d and 1 d for the flares observed in 2011 July and October, respectively (see Section 3), we obtain a size of $R \leq 7.6 \times 10^{16}$ and $R \leq 3.8 \times 10^{16}$ cm for the former and latter flare, respectively. These values are in agreement with what was found by the analysis of the spectral energy distribution during the high-activity states between 2008 and 2009 (D'Ammando et al. 2009; Abdo et al. 2010a).

The analysis of the data from the multifrequency monitoring campaigns obtained in the period considered in this paper showed that high activity was also observed at centimetre and millimetre wavelengths. In particular, the good time sampling at 22/23 GHz allowed us to identify several high-activity states, one almost simultaneous with the 2011 July γ-ray flare, when the flux density increased by about 60 per cent with respect to the minimum value measured in 2011 April. At lower radio frequencies no significant

flux density increase has been detected, while the lack of millimetre observations between 2011 June and September does not allow us to investigate the variability at higher frequencies. Interestingly, the 2011 July γ-ray flare seems to occur at the end of a 7-d period in which the optical EVPA rotates of about 380°. A similar behaviour was shown by 3C 279 during the strong γ-ray flare detected in 2009 February, which was accompanied by an abrupt change of the optical EVPA, while in radio no significant variability was observed (Abdo et al. 2010b).

An optical outburst was observed almost three weeks after the 2011 July γ-ray flare, when another high-activity γ-ray state was observed (Fig. 2). This outburst is also accompanied by an increase of both optical and radio polarization percentage, and a rotation of the optical EVPA of about 60° in 4 d. In contrast, no significant change in the radio EVPA has been noticed.

The most interesting feature shown by PKS 1510−089 is the huge radio flare observed since the beginning of 2011 September. Its multifrequency study indicates a rising stage, first detected above 23 GHz, and a decaying stage, as expected in the general shock model (e.g. Valtaoja et al. 1992). The exceptional γ-ray flare detected in 2011 October and the maximum in the millimetre light curves occur close in time, suggesting that the radio and γ-ray emission originates in the same region.

If the onset of the millimetre outburst is a consequence of the formation of a shock, then the γ-ray flare detected in October took place when the shock already moved downstream along the jet. The distance Δr between the region where the shock formed and the site responsible for the γ-ray emission may be determined by means of

$$\Delta r = \frac{\beta_{\rm app} c}{\sin\theta} \frac{\Delta t_{\rm obs}}{1+z}, \quad (2)$$

where $\beta_{\rm app}$ is the apparent jet velocity, c is the speed of light, $\Delta t_{\rm obs}$ is the time elapsed between the onset of the millimetre outburst and the γ-ray flare in the observer's frame, and θ is the viewing angle (Pushkarev, Kovalev & Lister 2010). In this case $\Delta t_{\rm obs}$ is about 40 d: $\Delta t_{\rm obs}$ is computed from the 22 GHz data between 2011 September 9, i.e. when the flux density doubled its value, and 2011 October 17, i.e. the detection of the γ-ray flare. If we assume $\beta_{\rm app} = 25.4$ (see Section 4.3), we find that the γ-ray flare is produced at a projected distance of ∼0.6 pc (i.e. 0.1 mas at the source redshift) from the site where the shock detected in the radio band was formed. If we consider $\theta = 3°$, as derived from previous studies of this source (e.g. Lister et al. 2009c; Abdo et al. 2010a; Marscher et al. 2010; D'Ammando et al. 2011; Orienti et al. 2011b), we find that the deprojected distance is about 10 pc. This result is in agreement with the idea that at least some γ-ray flares do not take place within the BLR. The parsec-scale distance of the site responsible for the γ-ray variability may be reconciled with the small size of the emitting region derived from equation (1), in the case the high-energy emission is due to turbulent plasma crossing a pre-existent standing shock, likely the radio core, located along the jet at several parsecs away from the nucleus (e.g. Marscher 2011). In this case, a contribution of synchrotron self-Compton (SSC) in addition to inverse Compton produced by scattering of the infrared photons from the dusty torus (e.g. Sikora, Moderski & Madejski 2008) may be at the origin of the γ-ray emission (e.g. Lähteenmäki & Valtaoja 2003; Marscher et al. 2010; Marscher 2011).

The multiwavelength variability of PKS 1510−089 during 2011 has some similarities with the radio-to-γ-ray outburst of the blazar BL Lacertae observed in 2005 (Marscher et al. 2008). Although the time sampling of both the radio and optical observations are not adequate for an accurate interpretation of the phenomena, we may speculate a possible connection between the two main γ-ray flares and the radio outburst of PKS 1510−089 in 2011, as it was done for BL Lacertae.

In both sources the first high-energy flare coincides with an abrupt rotation of the optical EVPA and the lack of significant flux density variability at the longer radio wavelengths. The rotation of the polarization angle suggests that the shock is likely produced by a disturbance of the flow at the beginning of the jet. The perturbed flow follows a spiral path as it propagates through the toroidal magnetic field of the initial part of the jet, i.e. the acceleration and collimation zone (Komissarov et al. 2007). A support to this interpretation comes from the decrease of the polarization percentage during the rotation, when the mean magnetic field of the disturbance is roughly transverse to the field of the unperturbed flow. The lack of significant radio counterpart indicates that this flare is taking place close to the central region of the AGN, where the radio emission is self-absorbed. As the perturbed flow propagates downstream the jet the opacity decreases, and the outburst becomes visible in the radio regime starting from the millimetre band down to longer wavelengths. The second high-energy flare would take place when the knot encounters a standing conical shock during its propagation along the jet. The perturbed flow would be compressed by its passage through the shock front. This would result in an amplification of the magnetic field and an enhancement of its emission. As the knot continues to propagate it becomes visible as a superluminal jet component detectable with the high-resolution VLBA observations. In this scenario both γ-ray flares would be produced by the same population of particles in two distinct moments (i.e. at distinct distances from the central engine) by means of different mechanisms.

5.2 The long-term variability of PKS 1510−089

The flaring activity shown by PKS 1510−089 since the launch of *AGILE* and *Fermi*-LAT has been characterized by several outbursts with different properties. In the period 2008 January to April, when intense activity was detected in the γ-ray, optical and millimetre regimes, no similar trend was found at the centimetre wavelengths (D'Ammando et al. 2009). A similar behaviour was found by D'Ammando et al. (2011) during the high-activity period at the beginning of 2009 March. Furthermore, during the flaring episodes occurred in 2009 January, the optical emission remained in a weak state (Marscher et al. 2010).

The flare detected in 2011 July, characterized by a higher γ-ray luminosity with respect to those previous outbursts, occurred close in time with a significant rotation of the optical EVPA, similar to what was observed in 2009 April. At 23 GHz there is a hint of flux density increase, but the lack of observations at higher frequencies does not allow us to reliably correlate the γ-ray variability with the light curves at lower frequencies, suggesting that opacity effects are dominant.

A different situation emerges from the strong γ-ray flares in 2008 September and 2009 April, which seem strictly related to the ejection of superluminal jet knots and increase of the flux density at high radio frequencies (Marscher et al. 2010; Orienti et al. 2011b). The strong flare in 2009 April is also associated with an exceptional optical flare, when it reached its historical peak with an *R*-band magnitude of about 13.6 (Larionov, Konstantinova & Blinov 2009) and a large rotation of the optical and radio polarization angle, indicating a common origin for the variability observed across the entire electromagnetic spectrum. This flaring episode is similar to the radio–γ-ray behaviour shown by the flare in 2011 October,

when the initial phase of the radio outburst seems to precede the high-energy variability. However, these episodes do not share all the same characteristics. Although the lack of optical information does not allow a complete multiband comparison, the polarimetric properties derived suggest a different behaviour between these two flares. In the first case, the increase of the radio flux density is accompanied by a drop in the fractional polarization and a rotation of about 90° of the EVPA. This behaviour is in agreement with a shock propagating perpendicular to the jet axis (Orienti et al. 2011b). On the other hand, in 2011 October the polarization percentage at 15 GHz reaches a minimum just before the γ-ray flare, and then increases as the emission switches from optically thick to optically thin at this frequency. However, the EVPA changes by only 20°, which is difficult to reconcile with the propagation of a transverse shock, but can be reproduced by an oblique shock. In this case, the expected variations in the polarization angle are strongly related to the obliqueness of the shock itself and to the characteristics of the magnetic field of the flow like its order and strength (Hughes et al. 2011).

6 CONCLUSIONS

In this paper, we presented results of the radio-to-γ-ray monitoring of PKS 1510−089 from 2010 November to 2012 January. Since 2011 July the source became very active at high energies, reaching its historical peak in γ rays in 2011 October.

A multifrequency analysis showed that the rapid and strong γ-ray flare detected in 2011 July is related to a rotation of the optical polarization angle suggesting a common region responsible for both γ-ray and optical emission. The lack of a simultaneous increase of the flux density in the centimetre regime suggests that the emitting region is close to the central AGN, at the beginning of the jet, where the radiation is opaque at the radio wavelengths.

On the other hand, the strong flare in 2011 October seems to be related to the huge radio outburst detected since the beginning of 2011 September starting from the higher radio frequencies. In this case, the radio outburst seems to precede the γ-ray flare, suggesting that the site responsible for the γ-ray emission is located along the jet, about 10 pc away from the central engine. This strong flare seems also related to the ejection of a new superluminal jet component from the radio core.

As in the case of BL Lacertae, both γ-ray flares may be interpreted by means of a single disturbance originated in the very initial part of the jet, opaque to the radio wavelength. As the perturbed flow propagates downstream the jet, the opacity decreases and the variability becomes visible at longer wavelengths. As the flow passes through a standing conical shock, which may be the radio core, its emission is amplified and a second high-energy flare is produced. In this case, the dominant emission mechanism may be either inverse Compton of infrared photons of the dusty torus or synchrotron photons from the standing shock. However, an SSC origin cannot be ruled out. Then, the disturbance continues its way downstream the jet becoming visible as a superluminal jet component by means of observations with the milliarcsecond resolution reached by the VLBI technique.

It is worth noting that during 2011 the γ-ray and optical light curves present additional high-activity states that complicate this simple picture. Furthermore, the long-term monitoring of PKS 1510−089 indicates that neither all the high-energy flares have an optical counterpart, like in the flaring episode occurring in 2009 January, nor all optical flares correspond to a γ-ray flare, as in the case of the 2011 January episode. Furthermore, the characteristics of the shocks may change among the various flaring episodes, producing different polarization properties as well as different light-curve behaviours at the various frequencies.

ACKNOWLEDGMENTS

Part of this work was done with the contribution of the Italian Ministry of Foreign Affairs and Research for the collaboration project between Italy and Japan. The VERA is operated by the National Astronomical Observatory of Japan. This work was partially supported by Grant-in-Aid for Scientific Researchers (24540240, MK) from Japan Society for the Promotion of Science (JSPS). The *Fermi*-LAT Collaboration acknowledges generous ongoing support from a number of agencies and institutes that have supported both the development and the operation of the LAT as well as scientific data analysis. These include the National Aeronautics and Space Administration and the Department of Energy in the United States, the Commissariat à l'Energie Atomique and the Centre National de la Recherche Scientifique / Institut National de Physique Nucléaire et de Physique des Particules in France, the Agenzia Spaziale Italiana and the Istituto Nazionale di Fisica Nucleare in Italy, the Ministry of Education, Culture, Sports, Science and Technology (MEXT), High Energy Accelerator Research Organization (KEK) and Japan Aerospace Exploration Agency (JAXA) in Japan, and the K. A. Wallenberg Foundation, the Swedish Research Council and the Swedish National Space Board in Sweden. Additional support for science analysis during the operations phase is gratefully acknowledged from the Istituto Nazionale di Astrofisica in Italy and the Centre National d'Études Spatiales in France.

This research is partly based on observations with the 100-m telescope of the MPIfR (Max-Planck-Institut für Radioastronomie) at Effelsberg and with the IRAM 30-m telescope. IRAM is supported by INSU/CNRS (France), MPG (Germany) and IGN (Spain). This research has made use of the data from the MOJAVE data base that is maintained by the MOJAVE team (Lister et al. 2009b). The OVRO 40-m monitoring programme is supported in part by NASA grants NNX08AW31G and NNX11A043G, and NSF grants AST-0808050 and AST-1109911. Part of the research is based on observations with the Medicina telescope operated by INAF – Istituto di Radioastronomia. We acknowledge the Enhanced Single-Dish Control System (ESCS) Development Team at the Medicina telescope.

Data from the Steward Observatory spectropolarimetric project were used. This programme is supported by Fermi Guest Investigator grants NNX08AW56G and NNX09AU10G. This research has made use of the NASA/IPAC Extragalactic Database NED which is operated by the JPL, Californian Institute of Technology, under contract with the National Aeronautics and Space Administration.

REFERENCES

Abdo A. A. et al., 2010a, ApJ, 721, 1425
Abdo A. A. et al., 2010b, Nat, 463, 919
Abdo A. A. et al., 2011c, ApJ, 733, L26
Ackermann M. et al., 2012, ApJS, 203, 4
Agudo I. et al., 2011a, ApJ, 726, L13
Agudo I. et al., 2011b, ApJ, 735, L10
Angelakis E., Fuhrmann L., Marchili N., Krichbaum T. P., Zensus J. A., 2008, MmSAI, 79, 1042
Atwood W. B. et al., 2009, ApJ, 697, 1071
Baars W. M., Genzel R., Pauliny-Toth I. I. K., Witzel A., 1977, A&A, 61, 99
Bachev R., Boeva S., Stoyanov K., Semkov E., 2011, The Astronomer's Telegram, 3479

Cortina J., 2012, The Astronomer's Telegram, 3965
D'Ammando F., Gasparrini D., 2011, The Astronomer's Telegram, 3473
D'Ammando F. et al., 2009, A&A, 508, 181
D'Ammando F. et al., 2011, A&A, 529, 145
Donnarumma I. et al., 2011, The Astronomer's Telegram, 3470
Fuhrmann L., Zensus J. A., Krichbaum T. P., Angelakis E., Readhead A. C. S., 2007, AIPC, 921, 249
Fuhrmann L. et al., 2008, A&A, 490, 1019
Gasparrini D., Cutini S., 2011, The Astronomer's Telegram, 3579
Hartman R. C. et al., 1999, ApJS, 123, 79
Hauser M., Lenain J. P., Wagner S., Hagen H., 2011, The Astronomer's Telegram, 3509
Hovatta T., Nieppola E., Tornikoski M., Valtaoja E., Aller M. F., Aller H. D., 2008, A&A, 485, 51
Hughes P. A., Aller M. F., Aller H. D., 2011, ApJ, 735, 81
Hungwe F., Dutka M., Ojha R., 2011, The Astronomer's Telegram, 3694
Jorstad S. G., Marscher A. P., Mattox J. R., Wehrle A. E., Bloom S. D., Yurchenko A. V., 2001, ApJS, 134, 181
Jorstad S. G. et al., 2005, AJ, 130, 1418
Komissarov S.S, Barkov M. V., Vlahakis N., Königl A., 2007, MNRAS, 380, 51
Kovalev Y. Y. et al., 2009, ApJ, 696, 17
Lähteenmäki A., Valtaoja E., 2003, ApJ, 590, 95
Landau R. et al., 1986, ApJ, 308, 78
Larionov V. M. et al., 2008, A&A, 492, 389
Larionov V. M., Konstantinova T. S., Blinov D. A., 2009, The Astronomer's Telegram, 2045
Leòn-Tavares J., Valtaoja E., Tornikoski M., Lähteenmäki A., Nieppola E., 2011, A&A, 532, 146
Lister M. L., Homan D. C., Kadler M., Kellermann K. I., Kovalev Y. Y., Ros E., Savolainen T., Zensus J. A., 2009a, ApJ, 696, L22
Lister M. et al., 2009b, AJ, 137, 3718
Lister M. L. et al., 2009c, AJ, 138, 1874
Marscher A. P., 2011, Fermi Symposium preprint (arXiv:1201.5402v1)
Marscher A. P., Gear W. K., 1985, ApJ, 298, 114
Marscher A. P. et al., 2008, Nat, 452, 966
Marscher A. P. et al., 2010, ApJ, 710, L126
Massaro E., Perri M., Giommi P., Nesci R., 2004, A&A, 413, 489
Mattox J. R. et al., 1996, ApJ, 461, 396
Nagai H. et al., 2012a, PASJ, (arXiv:1210.2469)
Nagai H. et al., 2012b, MNRAS, 423, L122
Nestoras I. et al., 2011, The Astronomer's Telegram, 3698
Nolan P. et al., 2012, ApJS, 199, 31
Orienti M., D'Ammando F., Giroletti M., Orlati A., 2011a, The Astronomer's Telegram, 3775
Orienti M., Venturi T., Dallacasa D., D'Ammando F., Giroletti M., Giovannini G., Vercellone S., Tavani M., 2011b, MNRAS, 417, 359
Pucella G. et al., 2008, A&A, 491, 21
Pushkarev A. B., Kovalev Y. Y., Lister M. L., 2010, ApJ, 722, 7
Richards J. L. et al., 2011, ApJS, 194, 29
Savolainen T., Homan D. C., Hovatta T., Kadler M., Kovalev Y. Y., Lister M. L., Ros E., Zensus J. A., 2010, A&A, 512, 24
Schinzel F. K., Lobanov A. P., Taylor G. B., Jorstad S. G., Marscher A. P., Zensus J. A., 2012, A&A, 537, 70
Sikora M., Moderski R., Madejski G. M., 2008, ApJ, 675, 71
Smith P. S., Montiel E., Rightley S., Turner J., Schmidt G. D., Jannuzi B. T., 2009, Fermi Symposium, eConf Proceedings C091122, (arXiv:0912.3621)
Striani E. et al., 2010, The Astronomer's Telegram, 2385
Tavecchio F., Ghisellini G., Bonnoli G., Ghirlanda G., 2010, MNRAS, 405, 94
Thompson D. J., Djorgovski S., de Carvalho R., 1990, PASP, 102, 1235
Tornikoski M., Valtaoja E., Teräsranta H., Smith A. G., Nair A. D., Clements S. D., Leacock R. J., 1994, A&A, 289, 673
Valtaoja E., Teräsranta H., Urpo S., Nesterov N. S., Laincia M., Valtonen M., 1992, A&A, 254, 71
Venturi T. et al., 2001, A&A, 379, 755
Wagner S., 2010, HEAD meeting, 11, 2706

This paper has been typeset from a TEX/LATEX file prepared by the author.